Dual Integrin and Gastrin-Releasing Peptide Receptor Targeted Tumor Imaging Using ^{18}F-labeled PEGylated RGD-Bombesin Heterodimer ^{18}F-FB-PEG$_3$-Glu-RGD-BBN

Zhaofei Liu,[§,†,‡] Yongjun Yan,[§,†] Frederic T. Chin,[†] Fan Wang,[‡] and Xiaoyuan Chen*[,†]

The Molecular Imaging Program at Stanford (MIPS), Department of Radiology, Biophysics, and Bio-X Program, Stanford University School of Medicine, Stanford, California 94305, Medical Isotopes Research Center, Peking University, Beijing, 100083, China

Received October 10, 2008

Radiolabeled RGD and bombesin peptides have been extensively investigated for tumor integrin $\alpha_v\beta_3$ and GRPR imaging, respectively. Due to the fact that many tumors are both integrin and GRPR positive, we designed and synthesized a heterodimeric peptide Glu-RGD-BBN, which is expected to be advantageous over the monomeric peptides for dual-receptor targeting. A PEG_3 spacer was attached to the glutamate α-amino group of Glu-RGD-BBN to enhance the ^{18}F labeling yield and to improve the in vivo kinetics. PEG_3-Glu-RGD-BBN possesses the comparable GRPR and integrin $\alpha_v\beta_3$ receptor-binding affinities as the corresponding monomers, respectively. The dual-receptor targeting properties of ^{18}F-FB-PEG_3-Glu-RGD-BBN were observed in PC-3 tumor model. ^{18}F-FB-PEG_3-Glu-RGD-BBN with high tumor contrast and favorable pharmacokinetics is a promising PET tracer for dual integrin and GRPR positive tumor imaging. This heterodimer strategy may also be an applicable method to develop other molecules with improved in vitro and in vivo characterizations for tumor diagnosis and therapy.

Introduction

Receptors that are uniquely expressed or markedly overexpressed in tumors have been the potential targets for cancer diagnosis and therapy. The ability to measure the receptor expression is of vital importance for making the accurate diagnosis, staging, restaging, patient stratification, and treatment response monitoring. In recent years, there has been a great acceleration in the development of radiolabeled receptor-binding peptides for single photon emission computed tomography (SPECT) and positron emission tomography (PET) imaging in nuclear oncology.[1,2]

Integrin $\alpha_v\beta_3$ is highly expressed on invasive tumors such as late-stage glioblastomas, breast and prostate tumors, malignant melanomas, and ovarian carcinomas as well as the new-born blood vessels.[3,4] The expression level of integrin $\alpha_v\beta_3$ is an important factor in determining the invasiveness and metastatic potential of malignancy in both preclinical animal models and cancer patients.[5] In the past few years, we and others have successfully developed a series RGD[a] peptide (Arg-Gly-Asp) radiotracers with favorable in vivo kinetics for tumor integrin $\alpha_v\beta_3$ imaging.[6−11] On the other hand, the gastrin-releasing peptide receptor (GRPR) has also been shown to be massively overexpressed in several human tumors, including breast cancer, prostate cancer, small cell lung cancer, ovarian cancer, endometrial cancers, and gastrointestinal stromal tumors.[12−14] Radiolabeled bombesin (BBN) and its analogues that specifically bind to GRPR have been extensively investigated for both diagnosis and treatment of GRPR-positive tumors.[15−19] ^{99m}Tc and ^{68}Ga labeled BBN analogues have also been tested in humans.[16,20]

During the processes of angiogenesis, invasion and metastasis of the GRPR-positive tumors, the activated endothelial cells around the tumor tissues would express high level of integrin $\alpha_v\beta_3$ and many GRPR-positive tumor cells are also integrin $\alpha_v\beta_3$-positive[21] so the tumors would be dual integrin and GRPR receptors positive. We have thus developed a BBN-RGD peptide heterodimer that recognizes both GRPR through the BBN motif and integrin $\alpha_v\beta_3$ through RGD motif. The ^{18}F-labeled BBN-RGD heterodimer exhibits excellent tumor uptake and favorable in vivo kinetics far superior to the BBN and RGD analogues in several prostate cancer xenograft models.[22] In that study, however, the peptide heterodimer was synthesized by coupling BBN and RGD with glutamate in solution phase. As the two carboxylate groups on the glutamic acid are asymmetric, two products are produced, namely Glu-BBN-RGD (RGD on the Glu side chain γ-position) and Glu-RGD-BBN (BBN on the Glu side chain γ-position), which are not separable by high performance liquid chromatography (HPLC). Moreover, the radiolabeling yield using *N*-succinimidyl-4-^{18}F-fluorobenzoate (^{18}F-SFB) as the synthon led to relatively low radiochemical yield presumably due to the steric hindrance and the relatively low reactivity of the glutamate α-amino group. In this study, we synthesized Glu-RGD-BBN by using Fmoc-Glu-OAll as an orthogonally protected building block (Scheme 1). We also inserted an PEG_3 spacer 11-amino-3,6,9-trioxaundecanoic acid onto the glutamate α-amino group of Glu-RGD-BBN to increase the overall hydrophilicity and to alleviate the steric hindrance,[23−25] thereby increasing the ^{18}F labeling yield. The titled compound ^{18}F-FB-PEG_3-Glu-RGD-BBN was then evaluated in human prostate cancer PC-3 tumor model for microPET and biodistribution studies.

Results

Chemistry and Radiochemistry. The Glu-RGD-BBN peptide heterodimer was synthesized stepwise by solid-phase

* To whom correspondence should be addressed. Phone: 650-725-0950. Fax: 650-736-7925. E-mail: shawchen@stanford.edu. Address: The Molecular Imaging Program at Stanford (MIPS), Department of Radiology and Bio-X Program, Stanford University School of Medicine, 1201 Welch Road, P095 Stanford, CA 94305-5484.

† The Molecular Imaging Program at Stanford (MIPS), Department of Radiology, Biophysics, and Bio-X Program, Stanford University School of Medicine.

‡ Medical Isotopes Research Center, Peking University.

§ Contributed equally to this work.

[a] Abbreviations: TFA, trifluoroacetic acid; PEG_3, PEG_3, 11-amino-3,6,9-trioxaundecanoic acid; GRPR, gastrin-releasing peptide receptor; DIPEA, *N*,*N*-diisopropylethylamine; TSTU, *O*-(*N*-succinimidyl)-1,1,3,3-tetramethyluronium tetrafluoroborate; DMF, *N*,*N*′-dimethylformamide; SFB, *N*-succinimidyl-4-fluorobenzoate; RGD, Arg-Gly-Asp (arginine-glycine-aspartic acid); BBN, bombesin.

10.1021/jm801285t CCC: $40.75
Published on Web 12/29/2008

Scheme 1. Synthesis of Glu-RGD-BBN[a]

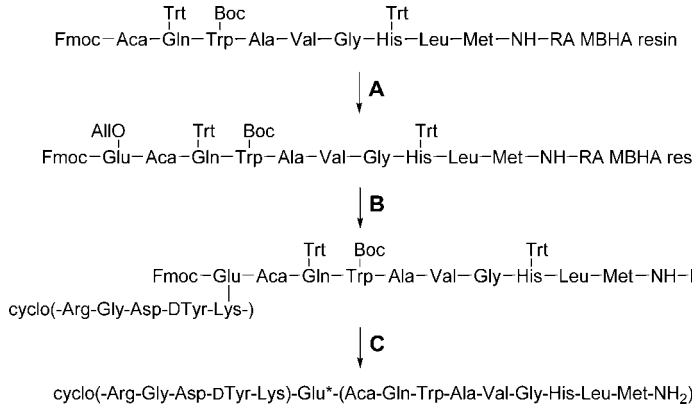

[a] The protected linear peptide was assembled on a Rink amide MBHA resin. (A) Removal of Fmoc protecting group and attachment of Fmoc-Glu-OAll where the α-carboxylate group was orthogonally protected as allyl ester. (B) Deprotection of OAll with $Pd(Ph_3P)_4/CHCl_3$/AcOH/NMM, activation of the α-carboxylate group on Glu with *O*-(*N*-succinimidyl)-1,1,3,3-tetramethyluronium tetrafluoroborate (TSTU), and coupling with cyclo(−Arg-Gly-Asp-DTyr-Lys−) through the Lys side chain ε-amine group. (C) Removal of Fmoc with piperidine and detaching/deprotecting the peptide with TFA/EDT/TIS to afford the Glu-RGD-BBN.

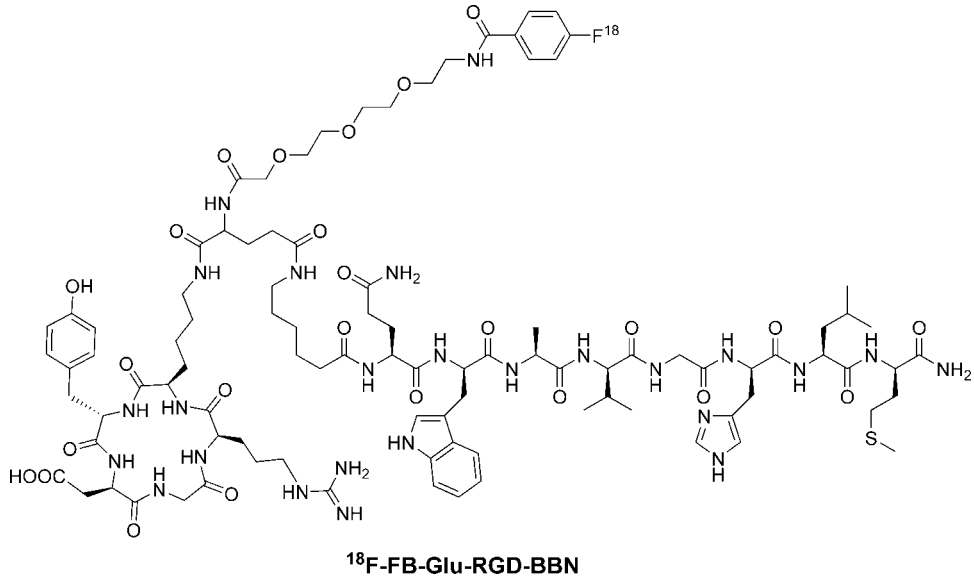

Figure 1. Chemical structure of ^{18}F-FB-PEG_3-Glu-RGD-BBN. The cyclic RGD peptide c(RGDyK) was connected with Aca-BBN(7−14) through a glutamate linker with RGD attached to the α-carboxylate and BBN attached to the γ-carboxylate. Labeling with ^{18}F was carried out via acylation of the amino group at the PEG_3 spacer using ^{18}F-SFB as synthon.

peptide synthesis method, illustrated in Scheme 1. PEG_3-Glu-RGD-BBN was synthesized following a previously reported procedure.[24] ^{18}F-FB-PEG_3-Glu-RGD-BBN (Figure 1) was prepared by coupling *N*-succinimidyl-4-^{18}F-fluorobenzoate (^{18}F-SFB) with PEG_3-Glu-RGD-BBN under slightly basic conditions at 60 °C for 30 min followed by HPLC purification. The radiochemical yield was 42% from ^{18}F-SFB with high radiochemical purity (>99%) (Supporting Information Figure S7). The effective specific activity was estimated to be 100 TBq/mmol on the basis of the labeling agent ^{18}F-SFB, as the unlabeled peptides were efficiently separated from the product.

Cell Binding Assay. The integrin $\alpha_v\beta_3$ receptor-binding affinities of cyclic RGD peptide c(RGDyK), PEG_3-Glu-RGD-BBN, and FB-PEG_3-Glu-RGD-BBN were determined by performing competitive binding assay using ^{125}I-c(RGDyK) as the radioligand. All peptides inhibited the binding of ^{125}I-c(RGDyK) to integrin expressing U87MG cells in a concentration-dependent manner. The IC_{50} values for c(RGDyK), PEG_3-Glu-RGD-BBN, and FB-PEG_3-Glu-RGD-BBN were 11.19 ± 1.44, 10.80 ± 1.46, and 13.77 ± 1.82 nM, respectively (Figure 2A). The binding affinities of Aca-BBN(7−14), PEG_3-Glu-RGD-BBN, and FB-PEG_3-Glu-RGD-BBN for GRPR were evaluated using GRPR positive PC-3 cells with ^{125}I-[Tyr^4]BBN as the radioligand. Results of the cell-binding assay were plotted in sigmoid curves for the displacement of ^{125}I-[Tyr^4]BBN from PC-3 cells as a function of increasing concentration of BBN analogues. The IC_{50} values were determined to be 78.96 ± 2.12 nM for BBN, 85.45 ± 1.95 nM for PEG_3-Glu-RGD-BBN, and 73.28 ± 1.57 nM for FB-PEG_3-Glu-RGD-BBN on PC-3 cells (Figure 2B). The comparable IC_{50} values from these two sets of experiments suggest that the incorporation of PEG_3 spacer to Glu-RGD-BBN peptide possesses comparable GRPR and integrin $\alpha_v\beta_3$ receptor-binding affinities as the corresponding unmodified monomers. Further coupling of 4-fluorobenzoyl group also had little effect on the integrin and GRPR receptor binding characteristics. The results obtained for Glu-RGD-BBN are slightly less affine to the previously reported BBN-RGD heterodimers synthesized in solution phase.[22]

Cell Uptake Studies. The cell uptake of ^{18}F-FB-PEG_3-Glu-RGD-BBN was evaluated in PC-3 tumor cells that express high

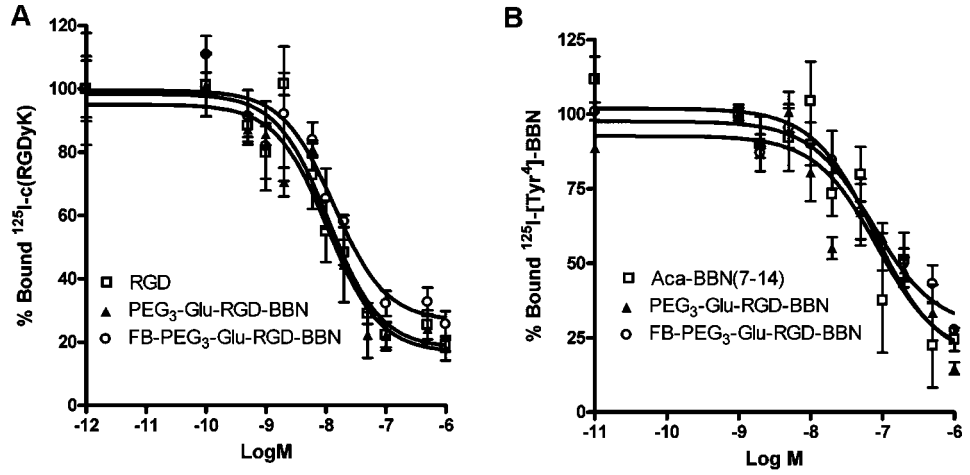

Figure 2. (A) Inhibition of ^{125}I-c(RGDyK) binding to integrin $\alpha_v\beta_3$ on U87MG cells by c(RGDyK), PEG$_3$-Glu-RGD-BBN, and FB-PEG$_3$-Glu-RGD-BBN: □, c(RGDyK) ($IC_{50} = 11.19 \pm 1.44$); ▲, PEG$_3$-Glu-RGD-BBN ($IC_{50} = 10.80 \pm 1.46$); ○, FB-PEG$_3$-Glu-RGD-BBN ($IC_{50} = 13.77 \pm 1.82$) ($n = 3$, mean ± SD). (B) Inhibition of ^{125}I-[Tyr^4]-BBN (GRPR-specific) binding to GRPR on PC-3 cells by Aca-BBN (7−14), PEG$_3$-Glu-RGD-BBN, and FB-PEG$_3$-Glu-RGD-BBN: □, Aca-BBN (7−14), ($IC_{50} = 78.96 \pm 2.12$); ▲, PEG$_3$-Glu-RGD-BBN ($IC_{50} = 85.45 \pm 1.95$); ○, FB-PEG$_3$-Glu-RGD-BBN ($IC_{50} = 73.28 \pm 1.57$) ($n = 3$, mean ± SD).

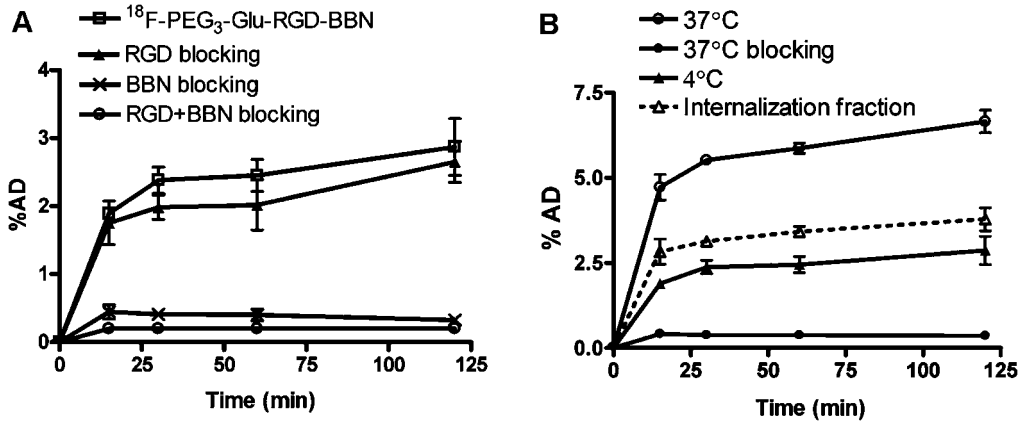

Figure 3. (A) Cell uptake assay of ^{18}F-FB-PEG$_3$-Glu-RGD-BBN on PC-3 tumor cells at 4 °C: □, without blocking; ▲, blocking with c(RGDyK); ×, blocking with Aca-BBN (7−14); ○, blocking with c(RGDyK) and Aca-BBN (7−14) ($n = 3$, mean ± SD). (B) Cell uptake assay of ^{18}F-FB-PEG$_3$-Glu-RGD-BBN on PC-3 tumor cells at 37 °C: ○, without blocking; ●, bhocking with Glu-RGD-BBN; ▲, cell uptake of ^{18}F-FB-PEG$_3$-Glu-RGD-BBN at 4 °C (for comparison); Δ, the internalized fraction of ^{18}F-FB-PEG$_3$-Glu-RGD-BBN (calculated by subtracting the cell uptake at 4 °C from the uptake at 37 °C at each time point) ($n = 3$, mean ± SD).

GRPR and moderate integrin levels. Figure 3A shows the results at 4 °C, in which the radiotracer only binds to the receptors on the cell surface without internalization. Rapid binding of ^{18}F-FB-PEG$_3$-Glu-RGD-BBN to the cell surface was observed for the first 15 min of incubation. After 15 min, the radiotracer exhibited a small and steady increase with time. Cell surface binding of ^{18}F-FB-PEG$_3$-Glu-RGD-BBN was partially inhibited in the presence of either RGD or Aca-BBN(7−14) peptide alone. The inhibition of BBN was more effective than RGD peptide. When both RGD and BBN were coincubated with ^{18}F-FB-PEG$_3$-Glu-RGD-BBN, the binding of ^{18}F-FB-PEG$_3$-Glu-RGD-BBN with PC-3 cells was significantly inhibited to trace level. For example, at 60 min, the cell uptake of ^{18}F-FB-PEG$_3$-Glu-RGD-BBN was inhibited by 17.55 ± 8.89%, 83.67 ± 2.09% and 91.97 ± 0.14% by RGD, BBN, and RGD + BBN, respectively (Figure 3A). The cell uptake of ^{18}F-FB-PEG$_3$-Glu-RGD-BBN was significantly increased when incubated at 37 °C due to both cell-surface receptor binding and receptor mediated internalization. As shown in the Figure 3B, the cell uptake of ^{18}F-FB-PEG$_3$-Glu-RGD-BBN was 4.72 ± 0.37%, 5.51 ± 0.11%, 5.87 ± 0.15%, and 6.65 ± 0.34% at 15, 30, 60, and 120 min, respectively. The cell uptake values of ^{18}F-FB-PEG$_3$-Glu-RGD-BBN are slightly higher than those of our previously reported ^{18}F-labeled BBN-RGD tracer that without the PEG3 spacer in the later time points.[22] The cell uptake was significantly inhibited by coincubation with excess amount of Glu-RGD-BBN peptide heterodimer, indicating the specific uptake of the radiotracer in PC-3 tumor cells. The internalized fraction was calculated by subtracting the cell uptake at 4 °C from the uptake at 37 °C at each time point (dotted line in Figure 3B). The internalized values were between the total uptake (37 °C) and the cell-surface binding (4 °C) at all time points. The internalization of ^{18}F-FB-PEG$_3$-Glu-RGD-BBN was rapid, reaching about 3.5% within 30 min of incubation, and plateaus afterward.

MicroPET Imaging. Representative coronal microPET images of PC-3 tumor-bearing mice ($n = 4$) at different times after intravenous injection of 3.7 MBq (100 μCi) of ^{18}F-FB-PEG$_3$-Glu-RGD-BBN are shown in Figure 4A. The tumors were clearly visible with high contrast to contralateral background at all time points measured from 30 to 120 min. Prominent uptake was also observed in the kidneys at early time points, suggesting that this tracer is mainly excreted through the renal route. Quantification of tumor and major organ activity accumulation in microPET scans was realized by measuring the

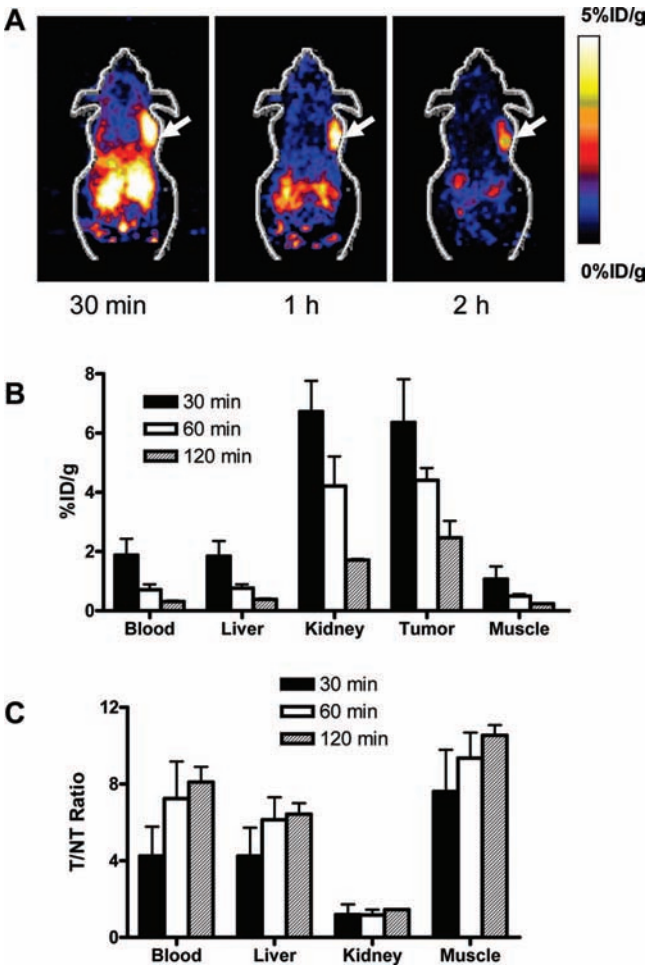

Figure 4. (A,B) The coronal microPET images and the radioactivity accumulation quantification in selected organs of the PC-3 tumor-bearing mice at 30, 60, and 120 min after injection of 3.7 MBq (100 μCi) of ^{18}F-FB-PEG$_3$-Glu-RGD-BBN. Arrows indicate the presence of PC-3 tumors. All microPET images were decay-corrected to the injection time. (C) Calculated tumor/nontumor (T/NT) ratios from (B).

regions of interest (ROIs) that encompass the entire organ on the coronal images. The tumor uptake of ^{18}F-FB-PEG$_3$-Glu-RGD-BBN was determined to be 6.35 ± 2.52, 4.41 ± 0.71, and 2.47 ± 0.81 %ID/g at 30, 60, and 120 min. The liver uptake was very low, the highest of which is less than 2%ID/g at 30 min postinjection (Figure 4B). With the rapid clearance of the tracer from normal nontargeted organs, the tumor/nontumor (T/NT) ratio increased with time. At 120 min postinjection, the T/NT ratios were 8.10 ± 1.14 for blood, 6.43 ± 0.81 for liver, 1.44 ± 0.05 for kidneys, and 10.54 ± 0.75 for muscle, respectively (Figure 4C). The T/NT ratios of ^{18}F-FB-PEG$_3$-Glu-RGD-BBN are all higher ($P < 0.05$) than those of the ^{18}F-FB-Glu-BBN-RGD tracer[22] at 1 and 2 h postinjection, which is consistent with our previous results that the PEGylation will improve the in vivo kinetics of the tracers.[7,23,24]

The integrin and GRPR dual-receptor binding specificity of ^{18}F-FB-PEG$_3$-Glu-RGD-BBN in vivo was conformed by several blocking studies (Figure 5). Representative coronal images of PC-3 tumor mice at 1 h postinjection of ^{18}F-FB-PEG$_3$-Glu-RGD-BBN in the presence of RGD (10 mg/kg of c(RGDyK)), BBN (15 mg/kg of Aca-BBN(7−14)), or both RGD and BBN (10 mg/kg of RGD and 15 mg/kg of BBN) are illustrated in Figure 5A. The tumor uptake ^{18}F-FB-PEG$_3$-Glu-RGD-BBN (Figure 5B) was partially inhibited by either RGD (2.19 ± 0.97 %ID/g, 50% decrease of tumor uptake, $n = 3$) or BBN (1.58 ± 0.52 %ID/g, 65% decrease of the tumor uptake, $n = 3$) alone. In contrast, when ^{18}F-FB-PEG$_3$-Glu-RGD-BBN was coadministered with both RGD and BBN, the tumor uptake was significant inhibited to the background level (0.43 ± 0.08%ID/g, 90% decrease of the tumor uptake, $n = 3$).

The tumor targeting efficacy of ^{18}F-FB-PEG$_3$-Glu-RGD-BBN in PC-3 tumor-bearing nude mice was also evaluated by 30 min dynamic microPET scanning followed by 5-min static scans at 1 and 2 h postinjection. As shown in Figure 6, the tracer cleared rapidly from the blood circulation (ROI at the heart). For example, the blood %ID/g at 30 min is only 35% of that at 2 min pi. The PC-3 tumor uptake was 3.54, 4.86, 5.64, 4.08, and 2.88 %ID/g at 5, 15, 30, 60, and 120 min pi, respectively. The tracer was excreted mainly through the kidneys. The kidney uptake reached a peak at about 10 min pi and then decreased with time. At 120 min pi, the tumor uptake of the tracer was higher than any of the other normal organ.

To validate the accuracy of microPET quantification, a biodistribution study was performed in nude mice bearing PC-3 tumors. Each mouse was injected with 0.74 MBq (20 μCi) of ^{18}F-FB-PEG$_3$-Glu-RGD-BBN and then sacrificed at 1 h pi ($n = 4$). As shown in Figure 7, the tumor uptake was 4.00 ± 0.08 %ID/g, and the kidney uptake was 4.87 ± 0.67 %ID/g. The uptake values in the blood, heart, liver, spleen, bone, and muscle were all less than 2%ID/g. ^{18}F-FB-PEG$_3$-Glu-RGD-BBN showed relatively high uptake in the normal organs that express GRPR, such as stomach, small intestine, and pancreas. Comparing the biodistribution and microPET quantification, there was no significant difference between the blood, liver, kidneys, tumor, and muscle ($P > 0.05$; Figure 7), suggesting that quantification of noninvasive microPET scans is a true reflection of the distribution of ^{18}F-FB-PEG$_3$-Glu-RGD-BBN in these organs. Note that the pancreas was unable to be delineated from microPET due to the limit of the spatial resolution.

Discussion

^{18}F ($t_{1/2} = 109.7$ min; β^+, 99%) is an ideal short-lived PET isotope for labeling small molecular recognition units, such as biologically active peptides, and is easily produced in the small biomedical cyclotrons. Most peptides have the N-terminal primary amine group and one or more lysine ε-amino residues that can be labeled with ^{18}F through an amine-reactive prosthetic labeling group such as ^{18}F-SFB.[9−11] ^{18}F-labeled RGD peptides have been synthesized and investigated for the imaging of tumor integrin $\alpha_v\beta_3$ expression in patients.[11] ^{18}F-Labeled bombesin peptides were also reported to be successful in imaging the GRPR-positive tumors.[15] In this study, we connected the monomeric RGD peptide with BBN through the glutamate linker. For easy labeling with ^{18}F and optimizing the in vivo kinetics, we also conjugated the Glu-RGD-BBN heterodimer with PEG$_3$. The in vitro and in vivo characterizations of the ^{18}F-FB-PEG$_3$-Glu-RGD-BBN heterodimer were investigated in a dual integrin $\alpha_v\beta_3$ and GRPR positive PC-3 tumor model.

In our previous studies, we observed that using ^{18}F-SFB as the synthon, the radiolabeling yield for the heterodimeric BBN-RGD peptide, is significantly lower than that for the monomeric BBN or RGD peptide, which was presumably due to the steric hindrance and relatively low reactivity of the glutamate α-amino group.[22] To overcome the problem of low labeling yield, we inserted a PEG$_3$ spacer between the α-amino of the glutamate in Glu-RGD-BBN heterodimer and the prosthetic ^{18}F-labeling group. The PEGylation is expected to decrease clearance rate, retain biologic activity, obtain a stable linkage, and enhance

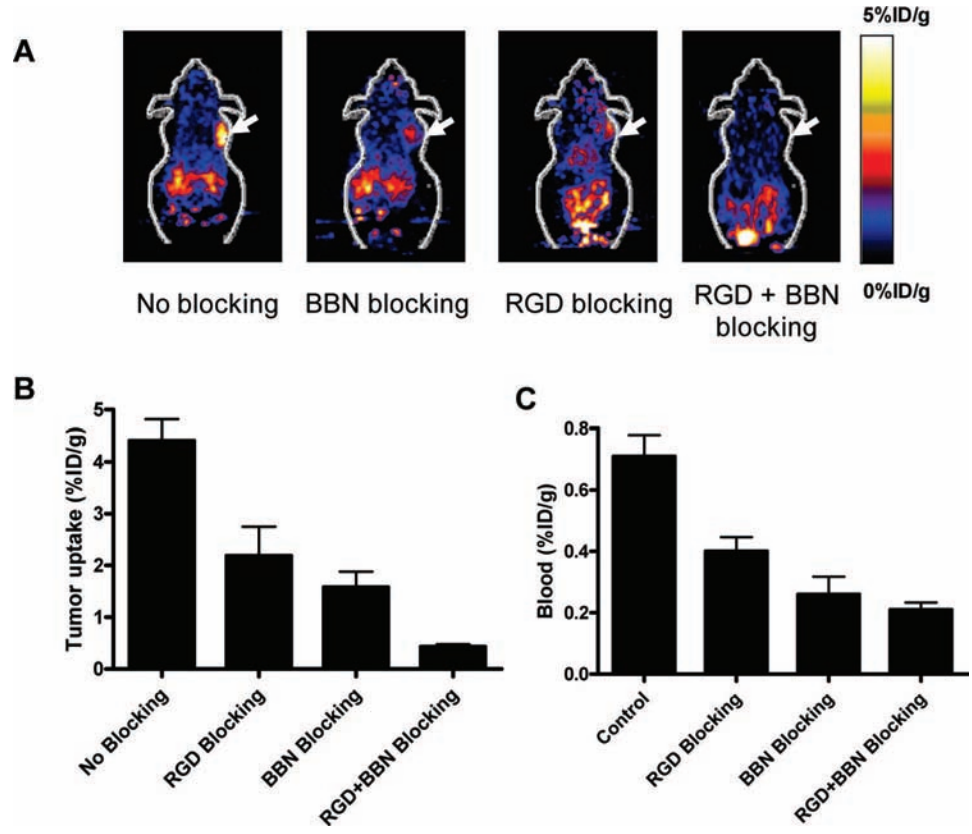

Figure 5. (A) Decay-corrected whole-body coronal microPET images of PC-3 tumor-bearing mice at 1 h after injection of 3.7 MBq (100 μCi) ^{18}F-FB-PEG$_3$-Glu-RGD-BBN and a blocking dose of c(RGDyK) (10 mg/kg of mouse body weight), BBN peptide (15 mg/kg mouse body weight), or RGD + BBN peptides (10 mg/kg for RGD and 15 mg/kg for BBN) ($n = 3$). (B,C) Comparison between uptake of ^{18}F-FB-PEG$_3$-Glu-RGD-BBN in PC-3 tumor (B) or blood (C) with or without preinjection of blocking dose of peptides (c(RGDyK), BBN peptide, or RGD + BBN peptides). ROIs are shown as %ID/g ± SD ($n = 3$).

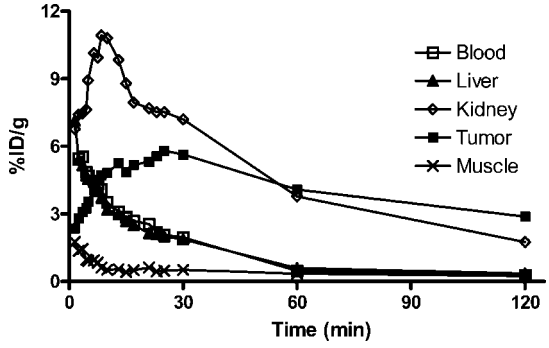

Figure 6. Time−activity curves of major organs in a PC-3 tumor-bearing nude mouse after intravenous injection of 3.7 MBq (100 μCi) ^{18}F-FB-PEG$_3$-Glu-RGD-BBN. Data were derived from a multiple time-point microPET study.

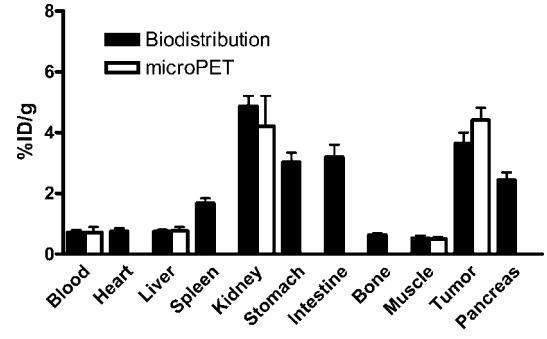

Figure 7. Biodistribution studies of ^{18}F-FB-PEG$_3$-Glu-RGD-BBN in PC-3 tumor-bearing nude mice at 1 h postinjection. The uptakes of ^{18}F-FB-PEG$_3$-Glu-RGD-BBN in PC-3 tumors and major organs measured by microPET and biodistribution were compared. Data are expressed as %ID/g ± SD ($n = 4$).

water solubility without significantly altering bioavailability.[24,26] Our receptor-binding assay data demonstrated that the binding affinity of PEG$_3$-Glu-RGD-BBN and FB-PEG$_3$-Glu-RGD-BBN is similar to Aca-BBN(7−14) for GRPR binding and is similar to c(RGDyK) for integin $\alpha_v\beta_3$ binding, indicating that the PEGylation did not affect the biological activities of RGD and BBN.

The in vitro cell uptake study at low temperature with no internalization of the radiotracer demonstrates that RGD and BBN can only partially inhibit the PC-3 cell uptake while RGD + BBN or Glu-RGD-BBN completely blocked the cell uptake of ^{18}F-FB-PEG$_3$-Glu-RGD-BBN (Figure 3A). This confirms the ability of ^{18}F-FB-PEG$_3$-Glu-RGD-BBN to bind both GRPR and integrin $\alpha_v\beta_3$ in cell culture. It is of note that BBN has more inhibitory ability than RGD when coincubated with ^{18}F-FB-PEG$_3$-Glu-RGD-BBN at 4 °C, which may be explained by the fact that PC-3 has much higher GRPR receptor density ($2.7 \pm 0.1 \times 10^6$ GRPRs per cell)[27] than integrin $\alpha_v\beta_3$ ($2.76 \pm 0.95 \times 10^3$ integrins per cell).[8] When the cells were incubated with ^{18}F-FB-PEG$_3$-Glu-RGD-BBN at 37 °C, more than half of the probes were internalized, which may be attributed totally via the BBN/GRPR recognition system because the internalization property of RGD is very low.[22]

We previously reported that the mixture of ^{18}F-FB-Glu-BBN-RGD (RGD on the Glu side chain γ-position) and ^{18}F-FB-Glu-RGD-BBN (BBN on the Glu side chain γ-position) exhibited much higher tumor uptake than ^{18}F-FB-RGD or ^{18}F-FB-BBN

alone and also higher than the sum of the two monomeric tracers at any time points tested.[22] As Glu-RGD-BBN and Glu-BBN-RGD are almost identical except that RGD and BBN are coupled to different carboxylates in the Glu linker, ^{18}F-FB-Glu-BBN-RGD and ^{18}F-FB-Glu-RGD-BBN are expected to have similar in vitro and in vivo behaviors. In this study, we used solid-phase synthesis method and prepared Glu-RGD-BBN. We also inserted a PEG_3 spacer for F-18 labeling. Comparison of the PET imaging results for ^{18}F-FB-PEG_3-Glu-RGD-BBN and ^{18}F-FB-Glu-RGD-BBN/^{18}F-FB-Glu-BBN-RGDN revealed that they have comparable tumor uptake and nonspecific tissue uptake, while the kidney uptake of ^{18}F-FB-PEG_3-Glu-RGD-BBN was appreciably lower. The PEG_3 spacer not only improved the radiolabeling yield for the RGD-BBN heterodimer but also contributed to a more rapid renal clearance of the ^{18}F-FB-PEG_3-Glu-RGD-BBN tracer.

The dual-receptor specificity of ^{18}F-FB-PEG_3-Glu-RGD-BBN in vivo was confirmed by several blocking studies. Both Aca-BBN(7−14) and cyclic RGD peptide c(RGDyK) can only partially inhibit the uptake of ^{18}F-FB-PEG_3-Glu-RGD-BBN in PC-3 tumor, as the BBN motif of the Glu-RGD-BBN can still bind to the GRPR when integrin is blocked by RGD, while the RGD motif of the Glu-RGD-BBN can bind to the integrin when GRPR is blocked by BBN. In accordance with the in vitro cell uptake experiment, BBN blocking of ^{18}F-FB-PEG_3-Glu-RGD-BBN is more effective than RGD peptide, presumably due to the fact that the PC-3 cells express a high level of GRPR but express a moderate level of integrin $\alpha_v\beta_3$. Interestingly, the blood uptake was also reduced after blocking with RGD, BBN, or both (Figure 5C). We assume that the blocking with excess nonradioactive peptides would result in less binding to normal organs that express the corresponding receptors and rapid wash out of ^{18}F-FB-PEG_3-Glu-RGD-BBN. This change of circulation half-life and normal organ/tissue binding can significantly affect the pharmacokinetics of ^{18}F-FB-PEG_3-Glu-RGD-BBN. For example, coinjection with RGD peptide will inhibit the integrin binding and ^{18}F-FB-PEG_3-Glu-RGD-BBN would only bind to GRPR, resulting in higher uptake in the GRPR positive intestines than that of nonblocking animals (Figure 5A).

Recently, other groups[28−31] also successfully synthesized heterodimer or hybrid peptides, which possessed dual-receptor binding property and synergistic bioactivities. We previously described the in vivo characterizations of ^{18}F-labeled PEGylated RGD homodimer peptide[24] in U87MG tumor model. Comparing with the RGD-BBN heterodimer tracer, the ^{18}F-labeled RGD homodimer peptides exhibited more promising tumor targeting property in the tumor model, which may be due to the extremely high integrin $\alpha_v\beta_3$ expression in the U87MG tumors. For the imaging of the lower integrin $\alpha_v\beta_3$-expressing but higher GRPR-expressing tumors (e.g, PC-3 tumor), the RGD-BBN heterodimer tracers should be more effective than the RGD homodimer because of the dual-receptor targeting property of the heterodimer. In the future, development of heterodimeric peptides that recognize other tumor targets that possess flexible linkers for simultaneous dual receptor binding may effectively increase the total affinity (avadity) of the tracers and eventually increase the tumor uptake. In addition, design of heteromultimeric tracers that recognize more tumor targets simultaneously is also worth further investigation for tumor imaging in the future.

Conclusion

In this study, we successfully designed and synthesized a dual integrin and GRPR receptor-binding heterodimeric peptide Glu-RGD-BBN by solid-phase peptide synthesis method. Glu-RGD-BBN possesses the comparable GRPR and integrin $\alpha_v\beta_3$ receptor-binding affinities as the corresponding Aca-BBN(7−14) and c(RGDyK) monomer, respectively. ^{18}F-labeled PEGylated Glu-RGD-BBN (^{18}F-FB-PEG_3-Glu-RGD-BBN) showed dual-receptor targeting properties both in vitro and in vivo. The high tumor uptake, good tumor-to-background contrast, and favorable pharmacokinetics of ^{18}F-FB-PEG_3-Glu-RGD-BBN warrant further investigation of this tracer in preclinical and clinical settings for dual integrin and GRPR positive tumor imaging. The heterodimer strategy may also provide a general method of developing peptide imaging and therapy molecules with improved in vitro and in vivo characterizations.

Experimental Section

General. All reagents, unless otherwise specified, were of analytical grade and commercially available. No-carrier added $^{18}F-F^-$ was obtained from an in-house cyclotron (GE Healthcare). The peptides Aca-BBN(7−14) and c(RGDyK) were synthesized by Peptides International. Boc-NH-PEG_3-COOH was purchased from Peptides International (Louisville, KY). The syringe filter and polyethersulfone membranes (pore size, 0.22 μm; diameter, 13 mm) were obtained from Nalge Nunc International. ^{125}I-[Tyr^4]BBN (74 TBq/mmol (2000 Ci/mmol)) were purchased from GE Healthcare, $Na^{125}I$ was purchased form Perkin-Elmer. Analytical as well as semipreparative reversed-phase high-performance liquid chromatography (RP-HPLC) was performed on a Dionex 680 chromatography system with a UVD 170U absorbance detector and model 105S single-channel radiation detector (Carroll & Ramsey Associates). The recorded data were processed using Chromeleon version 6.50 software. Isolation of peptides and ^{18}F-labeled peptides was performed using a Vydac protein and peptide column (218TP510; 5 μm, 250 mm × 10 mm). The flow was set at 5 mL/min using a gradient system starting from 95% solvent A (0.1% trifluoroacetic acid [TFA] in water) and 5% solvent B (0.1% TFA in acetonitrile [ACN]) (0−2 min) and ramped to 35% solvent A and 65% solvent B at 32 min. The analytic HPLC was performed using the same gradient system but with a Vydac column (218TP54, 5 μm, 250 mm × 4.6 mm) and a flow of 1 mL/min. The ultraviolet (UV) absorbance was monitored at 218 nm and the identification of the peptides was confirmed based on the UV spectrum acquired using a photodiode array detector.

Synthesis of Glu-RGD-BBN. The Glu-RGD-BBN peptide heterodimer was synthesized via solid-phase peptide synthesis strategy as described in Scheme 1. Loading of Fmoc-Met-Rink amide MBHA resin, synthesis of the bombesin peptide follows standard peptide synthesis protocols. Side chain protection was trityl (Trt) for histidine (His) and glutamine (Gln) and *tert*-butoxycarbonyl (Boc) for tryptophan (Trp). After loading Fmoc-Glu-OAll onto Aca, the α-allyl ester was then removed by treatment with $Pd(Ph_3P)_4$/$CHCl_3$/AcOH/NMM. The α-carboxylate was activated and coupled with cyclic RGD peptide cyclo(Arg-Gly-Asp-D-Tyr-Lys) (RGD) via the lysine side chain ε-amine group. After removing the Fmoc from Glu, the final peptide cyclo(Arg-Gly-Asp-D-Tyr-Lys)-Glu*-(Aca-Gln-Trp-Ala-Val-Gly-His-Leu-Met-NH_2) (Glu-RGD-BBN, * indicates the amino acid that links the RGD and BBN peptides and has a NH_2 group for PEG_3 conjugation, RGD is coupled to the Glu α-carboxylate group and BBN is coupled to the Glu side chain γ-carboxylate group) was obtained by detaching/deprotecting the Rink amide MBHA resin using 95% TFA in dichloromethane (DCM) plus ethandithiol (EDT) and triisopropylsilane (TIS) as scavengers. ES-MS: m/z 1783.9 for $[M + H]^+$ ($C_{81}H_{123}N_{24}O_{20}S$, calcd 1783.9). RP-HPLC R_t = 18.6 min.

Synthesis of PEG_3-Glu-RGD-BBN. To a solution of Boc-11-amino-3,6,9-trioxaundecanoic acid (Boc-NH-PEG_3-COOH, 40 mg, 0.13 mmol) and *N*,*N*-diisopropylethylamine (DIPEA, 20 μL) in ACN was added *O*-(*N*-succinimidyl)-1,1,3,3-tetramethyl-uronium tetrafluoroborate (TSTU, 27 mg, 0.09 mmol). The reaction mixture was stirred at room temperature for 0.5 h and then added to a

solution of Glu-RGD-BBN (36 mg, 0.02 mmol) in *N*,*N*′-dimethylformamide (DMF). After being stirred at room temperature for 2 h, the Boc-protected PEG$_3$-Glu-RGD-BBN was isolated by preparative HPLC. The Boc group was then removed with anhydrous TFA and the crude product was again purified by preparative HPLC. The collected fractions were combined and lyophilized to afford 23 mg of PEG$_3$-Glu-RGD-BBN as a white fluffy powder (yield: 58%). (MALDI-TOF MS: *m*/*z* 1973.3 for $[M + H]^+$ ($C_{89}H_{138}N_{25}O_{24}S$, calcd 1974.3)). RP-HPLC R_t = 18.8 min.

Synthesis of FB-PEG$_3$-Glu-RGD-BBN. *N*-Succinimidyl-4-fluorobenzoate (SFB, 4 mg, 16.8 μmol) and PEG$_3$-Glu-RGD-BBN (2 mg, 1.0 μmol) were mixed in 0.05 mol/L borate buffer (pH 8.5) at room temperature. After constant shaking for 2 h, the desired product FB-PEG$_3$-Glu-RGD-BBN was isolated by semipreparative HPLC (1.6 mg, yield: 76%). Analytical HPLC (RP-HPLC R_t = 23.3 min) and mass spectrometry (MALDITOF-MS: *m*/*z* 2095.9 for $[M + H]^+$ ($C_{96}H_{141}FN_{25}O_{25}S$, calcd 2095.4)) analyses confirmed the product identification.

Radiochemistry. *N*-Succinimidyl-4-^{18}F-fluorobenzoate (^{18}F-SFB) was synthesized and purified with HPLC as we previously reported by modifying GE TRACERlab FX-FN module. The purified ^{18}F-SFB was rotary evaporated to dryness, redissolved in dimethyl sulfoxide (DMSO, 200 μL), and added to a DMSO solution of PEG$_3$-Glu-RGD-BBN peptide (200 μg) and DIPEA (20 μL). The reaction mixture was incubated at 60 °C for 30 min. After dilution with 5% aqueous acetic acid solution (3 mL), the mixture was purified by semipreparative HPLC. The desired fractions containing ^{18}F-FB-PEG$_3$-RGD-BBN were combined and rotary evaporated to dryness. The activity was then reconstituted in PBS and analyzed with HPLC under the condition of: Vydac column (218TP54, 5 μm, 250 mm × 4.6 mm); eluent: (0.1% TFA in ACN):(0.1% TFA in H_2O) = 28:72; flow rate: 1 mL/min. The product was then passed through a 0.22 μm Millipore filter into a sterile multidose vial for in vitro and in vivo experiments.

Cell Line and Animal Models. The PC-3 human prostate carcinoma cell line was purchased from the American Type Culture Collection (ATCC, Manassas, VA). PC-3 cells were grown in F-12K nutrient mixture (Kaighn's modification) supplemented with 10% (v/v) fetal bovine serum (Invitrogen) at 37 °C with 5% CO_2. The PC-3 tumor model was generated by subcutaneous injection of 5×10^6 tumor cells into the right front flank of male athymic nude mice (Harlan). The mice were used for microPET studies when the tumor volume reached 100−300 mm^3 (3−4 wk after inoculation). All the animal procedures were performed according to a protocol approved by the Stanford University Institutional Animal Care and Use Committee.

Cell Binding Assay. We labeled c(RGDyK) with Na^{125}I and purified it with HPLC according to our previously described method.[32] The ^{125}I-c(RGDyK) was prepared in high specific activity (−1200 Ci/mmol). In vitro integrin $\alpha_v\beta_3$-binding affinities and specificities of PEG$_3$-Glu-RGD-BBN and FB-PEG$_3$-Glu-RGD-BBN were compared with c(RGDyK) via displacement cell-binding assays using ^{125}I-c(RGDyK) as the integrin-specific radioligand. Experiments were performed on integrin $\alpha_v\beta_3$ expressing U87MG human glioblastoma cells as we previously described.[33,34] In vitro GRPR binding affinities and specificities of PEG$_3$-Glu-RGD-BBN and FB-PEG$_3$-Glu-RGD-BBN were compared with Aca-BBN(7−14) via displacement cell-binding assays using ^{125}I-[Tyr^4]BBN as the radioligand. Experiments were performed on GRPR expressing PC-3 cells using the method we previously described. The best-fit 50% inhibitory concentration (IC_{50}) values were calculated by fitting the data with nonlinear regression using Graph Pad Prism (GraphPad Software, Inc.). Experiments were performed twice with triplicate samples.

Cell Uptake Studies. The cell uptake studies were performed as we previous described with some modifications.[22,27,35] Briefly, PC-3 cells were seeded into 12-well plates at a density of 5×10^5 cells per well and incubated overnight before experiments. After rinsing three times with PBS, cells were incubated with ^{18}F-FB-PEG$_3$-Glu-RGD-BBN (~0.3 μCi/well, in culture medium) with or without excess of cold RGD, BBN, or RGD-BBN (1 μmol/L) at 37 or 4 °C for 15, 30, 60, and 120 min. Tumor cells were then washed three times with chilled PBS and harvested by trypsinization with 0.25% trypsin/0.02% EDTA (Invitrogen Corp.). The cells suspensions were collected and measured in a γ counter (Packard, Meriden, CT). The cell uptake was expressed as the percent added radioactivity. Experiments were performed twice with triplicate wells.

MicroPET Imaging. PET scans and image analysis were performed using a microPET R4 rodent model scanner (Siemens Medical Solutions) as previously reported.[8,15] Each PC-3 tumor-bearing mouse was tail vein injected with about 3.7 MBq (100 μCi) of ^{18}F-FB-PEG$_3$-RGD-BBN under isoflurane anesthesia. Then 5 min static PET images were acquired at 30 min, 1 and 2 h post injection (pi) (n = 4). For dynamic scanning, 3.7 MBq (100 μCi) of ^{18}F-FB-PEG$_3$-RGD-BBN was tail vein injected in to one PC-3 tumor-bearing mouse. The 35 min dynamic scan (1 × 30 s, 4 × 1 min, 1 × 1.5 min, 4 × 2 min, 1 × 2.5 min, 4 × 3 min, total of 15 frames) was started 1 min after injection, and the 1 and 2 h time points static scans were also acquired after the 35 min dynamic scan. The images were reconstructed by a two-dimensional ordered-subsets expectation maximum (OSEM) algorithm, and no correction was applied for attenuation or scatter. For the blocking experiment, the tumor mice were coinjected with 10 mg/kg mouse body weight of c(RGDyK), Aca-bbn (7−14) (15 mg/kg), or both RGD and BBN (10 mg/kg and 15 mg/kg, respectiviely) and 3.7 MBq of ^{18}F-FB-PEG$_3$-RGD-BBN, and 5 min static PET scans were then acquired at 1 h pi (n = 3). For each microPET scan, regions of interests (ROIs) were drawn over each tumor, normal tissue, and major organs by using vendor software ASI Pro 5.2.4.0 on decay-corrected whole-body coronal images. The maximum radioactivity concentration (accumulation) within a tumor or an organ was obtained from mean pixel values within the multiple ROI volume, which were converted to MBq/mL/min by using a conversion factor. Assuming a tissue density of 1 g/mL, the ROIs were converted to MBq/g/min and then divided by the administered activity to obtain an imaging ROI-derived %ID/g.

Biodistribution Studies. Male athymic nude mice bearing PC-3 xenografts were injected with 0.74 MBq (20 μCi) of ^{18}F-FB-PEG$_3$-RGD-BBN to evaluate the distribution of the tracer in the tumor tissues and major organs of mice. All mice were sacrificed and dissected at 1 h after injection of the tracer. Blood, tumor, major organs, and tissues were collected and wet-weighed. The radioactivity in the tissue was measured by γ counter (Packard, Meriden, CT). The results were presented as percentage injected dose per gram of tissue (%ID/g). For each mouse, the radioactivity of the tissue samples was calibrated against a known aliquot of the injectate and normalized to a body mass of 20 g. Values were expressed as mean ± SD for a group of four animals (n = 4).

Statistical Analysis. Quantitative data were expressed as mean ± SD. Means were compared using one-way analysis of variance (ANOVA) and Student-s t test. P values <0.05 were considered statistically significant.

Acknowledgment. This work was supported, in part, by the National Cancer Institute (NCI; R01 120188, R01 CA119053, R21 CA121842, R21 CA102123, P50 CA114747, U54 CA119367, and R24 CA93862) and the Department of Defense (DOD; W81XWH-07-1-0374, W81XWH-04-1-0697, W81XWH-06-1-0665, W81XWH-06-1-0042). We thank Drs. Zibo Li and Kai Chen for their kind technical support and also thank the cyclotron team at Stanford University for ^{18}F-F$^-$ production. Z. Liu acknowledges the China Scholarship Council (CSC) for partly financial support during his visit to Stanford University.

Supporting Information Available: Analytical data for Glu-RGD-BBN, PEG$_3$-Glu-RGD-BBN, FB-PEG$_3$-Glu-RGD-BBN, and ^{18}F-FB-PEG$_3$-Glu-RGD-BBN. This material is available free of charge via the Internet at http://pubs.acs.org.

References

(1) Mankoff, D. A.; Link, J. M.; Linden, H. M.; Sundararajan, L.; Krohn, K. A. Tumor receptor imaging. *J. Nucl. Med.* **2008**, *49*, 149S–163S.

(2) Okarvi, S. M. Peptide-based radiopharmaceuticals: future tools for diagnostic imaging of cancers and other diseases. *Med. Res. Rev.* **2004**, *24* (3), 357–397.

(3) Hynes, R. O. Integrins: versatility, modulation, and signaling in cell adhesion. *Cell* **1992**, *69* (1), 11–25.

(4) Seftor, R. E.; Seftor, E. A.; Gehlsen, K. R.; Stetler-Stevenson, W. G.; Brown, P. D.; Ruoslahti, E.; Hendrix, M. J. Role of the $\alpha v\beta 3$ integrin in human melanoma cell invasion. *Proc. Natl. Acad. Sci. U.S.A* **1992**, *89* (5), 1557–1561.

(5) Brooks, P. C.; Clark, R. A.; Cheresh, D. A. Requirement of vascular integrin alpha v beta 3 for angiogenesis. *Science* **1994**, *264* (5158), 569–571.

(6) Chen, X.; Park, R.; Shahinian, A. H.; Tohme, M.; Khankaldyyan, V.; Bozorgzadeh, M. H.; Bading, J. R.; Moats, R.; Laug, W. E.; Conti, P. S. ^{18}F-labeled RGD peptide: initial evaluation for imaging brain tumor angiogenesis. *Nucl. Med. Biol.* **2004**, *31* (2), 179–189.

(7) Chen, X.; Sievers, E.; Hou, Y.; Park, R.; Tohme, M.; Bart, R.; Bremner, R.; Bading, J. R.; Conti, P. S. Integrin $\alpha v\beta 3$-targeted imaging of lung cancer. *Neoplasia* **2005**, *7* (3), 271–279.

(8) Zhang, X.; Xiong, Z.; Wu, Y.; Cai, W.; Tseng, J. R.; Gambhir, S. S.; Chen, X. Quantitative PET imaging of tumor integrin $\alpha v\beta 3$ expression with ^{18}F-FRGD2. *J. Nucl. Med.* **2006**, *47* (1), 113–121.

(9) Beer, A. J.; Niemeyer, M.; Carlsen, J.; Sarbia, M.; Nahrig, J.; Watzlowik, P.; Wester, H. J.; Harbeck, N.; Schwaiger, M. Patterns of $\alpha v\beta 3$ expression in primary and metastatic human breast cancer as shown by ^{18}F-Galacto-RGD PET. *J. Nucl. Med.* **2008**, *49* (2), 255–259.

(10) Beer, A. J.; Grosu, A. L.; Carlsen, J.; Kolk, A.; Sarbia, M.; Stangier, I.; Watzlowik, P.; Wester, H. J.; Haubner, R.; Schwaiger, M. [^{18}F]galacto-RGD positron emission tomography for imaging of alphavbeta3 expression on the neovasculature in patients with squamous cell carcinoma of the head and neck. *Clin. Cancer Res.* **2007**, *13* (22 Pt 1), 6610–6616.

(11) Haubner, R.; Weber, W. A.; Beer, A. J.; Vabuliene, E.; Reim, D.; Sarbia, M.; Becker, K. F.; Goebel, M.; Hein, R.; Wester, H. J.; Kessler, H.; Schwaiger, M. Noninvasive visualization of the activated $\alpha v\beta 3$ integrin in cancer patients by positron emission tomography and [^{18}F]Galacto-RGD. *PLoS Med.* **2005**, *2* (3), e70.

(12) Gugger, M.; Reubi, J. C. Gastrin-releasing peptide receptors in non-neoplastic and neoplastic human breast. *Am. J. Pathol.* **1999**, *155* (6), 2067–2076.

(13) Markwalder, R.; Reubi, J. C. Gastrin-releasing peptide receptors in the human prostate: relation to neoplastic transformation. *Cancer Res.* **1999**, *59* (5), 1152–1159.

(14) Scheffel, U.; Pomper, M. G. PET imaging of GRP receptor expression in prostate cancer. *J. Nucl. Med.* **2004**, *45* (8), 1277–1278.

(15) Zhang, X.; Cai, W.; Cao, F.; Schreibmann, E.; Wu, Y.; Wu, J. C.; Xing, L.; Chen, X. ^{18}F-labeled bombesin analogs for targeting GRP receptor-expressing prostate cancer. *J. Nucl. Med.* **2006**, *47* (3), 492–501.

(16) Dimitrakopoulou-; Strauss, A.; Hohenberger, P.; Haberkorn, U.; Macke, H. R.; Eisenhut, M.; Strauss, L. G. ^{68}Ga-labeled bombesin studies in patients with gastrointestinal stromal tumors: comparison with ^{18}F-FDG. *J. Nucl. Med.* **2007**, *48* (8), 1245–1250.

(17) Cescato, R.; Maina, T.; Nock, B.; Nikolopoulou, A.; Charalambidis, D.; Piccand, V.; Reubi, J. C. Bombesin receptor antagonists may be preferable to agonists for tumor targeting. *J. Nucl. Med.* **2008**, *49* (2), 318–326.

(18) Garrison, J. C.; Rold, T. L.; Sieckman, G. L.; Naz, F.; Sublett, S. V.; Figueroa, S. D.; Volkert, W. A.; Hoffman, T. J. Evaluation of the pharmacokinetic effects of various linking group using the ^{111}In-DOTA-X-BBN(7−14)NH2 structural paradigm in a prostate cancer model. *Bioconjugate Chem.* **2008**, *19* (9), 1803–1812.

(19) Zhang, H.; Chen, J.; Waldherr, C.; Hinni, K.; Waser, B.; Reubi, J. C.; Maecke, H. R. Synthesis and evaluation of bombesin derivatives on the basis of pan-bombesin peptides labeled with indium-111, lutetium-177, and yttrium-90 for targeting bombesin receptor-expressing tumors. *Cancer Res.* **2004**, *64* (18), 6707–6715.

(20) Van de Wiele, C.; Phonteyne, P.; Pauwels, P.; Goethals, I.; Van den Broecke, R.; Cocquyt, V.; Dierckx, R. A. Gastrin-releasing peptide receptor imaging in human breast carcinoma versus immunohistochemistry. *J. Nucl. Med.* **2008**, *49* (2), 260–264.

(21) Cooper, C. R.; Chay, C. H.; Pienta, K. J. The role of $\alpha v\beta 3$ in prostate cancer progression. *Neoplasia* **2002**, *4* (3), 191–194.

(22) Li, Z. B.; Wu, Z.; Chen, K.; Ryu, E. K.; Chen, X. ^{18}F-labeled BBN-RGD heterodimer for prostate cancer imaging. *J. Nucl. Med.* **2008**, *49* (3), 453–461.

(23) Chen, X.; Park, R.; Hou, Y.; Khankaldyyan, V.; Gonzales-Gomez, I.; Tohme, M.; Bading, J. R.; Laug, W. E.; Conti, P. S. MicroPET imaging of brain tumor angiogenesis with ^{18}F-labeled PEGylated RGD peptide. *Eur. J. Nucl. Med. Mol. Imaging* **2004**, *31* (8), 1081–1089.

(24) Wu, Z.; Li, Z. B.; Cai, W.; He, L.; Chin, F. T.; Li, F.; Chen, X. ^{18}F-labeled mini-PEG spacered RGD dimer (^{18}F-FPRGD2): synthesis and microPET imaging of $\alpha v\beta 3$ integrin expression. *Eur. J. Nucl. Med. Mol. Imaging* **2007**, *34* (11), 1823–1831.

(25) Wu, Z.; Li, Z. B.; Chen, K.; Cai, W.; He, L.; Chin, F. T.; Li, F.; Chen, X. microPET of tumor integrin $\alpha v\beta 3$ expression using ^{18}F-labeled PEGylated tetrameric RGD peptide (^{18}F-FPRGD4). *J. Nucl. Med.* **2007**, *48* (9), 1536–1544.

(26) Walsh, S.; Shah, A.; Mond, J. Improved pharmacokinetics and reduced antibody reactivity of lysostaphin conjugated to polyethylene glycol. *Antimicrob. Agents Chemother.* **2003**, *47* (2), 554–558.

(27) Yang, Y. S.; Zhang, X.; Xiong, Z.; Chen, X. Comparative in vitro and in vivo evaluation of two ^{64}Cu-labeled bombesin analogs in a mouse model of human prostate adenocarcinoma. *Nucl. Med. Biol.* **2006**, *33* (3), 371–380.

(28) Capello, A.; Krenning, E. P.; Bernard, B. F.; Breeman, W. A.; Erion, J. L.; de Jong, M. Anticancer activity of targeted proapoptotic peptides. *J. Nucl. Med.* **2006**, *47* (1), 122–129.

(29) Capello, A.; Krenning, E. P.; Bernard, B. F.; Breeman, W. A.; van Hagen, M. P.; de Jong, M. Increased cell death after therapy with an Arg-Gly-Asp-linked somatostatin analog. *J. Nucl. Med.* **2004**, *45* (10), 1716–1720.

(30) Bernard, B.; Capello, A.; van Hagen, M.; Breeman, W.; Srinivasan, A.; Schmidt, M.; Erion, J.; van Gameren, A.; Krenning, E.; de Jong, M. Radiolabeled RGD-DTPA-Tyr3-octreotate for receptor-targeted radionuclide therapy. *Cancer Biother. Radiopharm.* **2004**, *19* (2), 173–180.

(31) Vagner, J.; Xu, L.; Handl, H. L.; Josan, J. S.; Morse, D. L.; Mash, E. A.; Gillies, R. J.; Hruby, V. J. Heterobivalent ligands crosslink multiple cell-surface receptors: the human melanocortin-4 and delta-opioid receptors. *Angew. Chem., Int. Ed.* **2008**, *47* (9), 1685–1688.

(32) Chen, X.; Park, R.; Shahinian, A. H.; Bading, J. R.; Conti, P. S. Pharmacokinetics and tumor retention of ^{125}I-labeled RGD peptide are improved by PEGylation. *Nucl. Med. Biol.* **2004**, *31* (1), 11–19.

(33) Li, Z. B.; Cai, W.; Cao, Q.; Chen, K.; Wu, Z.; He, L.; Chen, X. ^{64}Cu-labeled tetrameric and octameric RGD peptides for small-animal PET of tumor $\alpha v\beta 3$ integrin expression. *J. Nucl. Med.* **2007**, *48* (7), 1162–1171.

(34) Li, Z. B.; Chen, K.; Chen, X. ^{68}Ga-labeled multimeric RGD peptides for microPET imaging of integrin $\alpha v\beta 3$ expression. *Eur. J. Nucl. Med. Mol. Imaging* **2008**, *35* (6), 1100–1108.

(35) Chen, X.; Park, R.; Hou, Y.; Tohme, M.; Shahinian, A. H.; Bading, J. R.; Conti, P. S. microPET and autoradiographic imaging of GRP receptor expression with ^{64}Cu-DOTA-[Lys^3]bombesin in human prostate adenocarcinoma xenografts. *J. Nucl. Med.* **2004**, *45* (8), 1390–1397.

JM801285T